Change of outgassing pattern of 67P/Churyumov–Gerasimenko during the March 2016 equinox as seen by ROSINA

Sébastien Gasc,[1]⋆ Kathrin Altwegg,[1,2] Hans Balsiger,[1] Jean-Jacques Berthelier,[3] André Bieler,[4] Ursina Calmonte,[1] Björn Fiethe,[5] Stephen Fuselier,[6,7] André Galli,[1] Tamas Gombosi,[4] Margaux Hoang,[8,9] Johan De Keyser,[10] Axel Korth,[11] Léna Le Roy,[1] Urs Mall,[11] Henri Rème,[8,9] Martin Rubin,[1] Thierry Sémon,[1] Chia-Yu Tzou,[1] Jack Hunter Waite[6] and Peter Wurz[1,2]

[1]*Physikalisches Institut, University of Bern, CH-3012 Bern, Switzerland*
[2]*Center for Space and Habitability, University of Bern, CH-3012 Bern, Switzerland*
[3]*LATMOS, F-94100 Saint-Maur, France*
[4]*Department of Climate and Space Sciences and Engineering, University of Michigan, Ann Arbor, MI 48109, USA*
[5]*Institute of Computer and Network Engineering (IDA), TU Braunschweig, D-38106 Braunschweig, Germany*
[6]*Space Science and Engineering Division, Southwest Research Institute, San Antonio, TX 78228, USA*
[7]*University of Texas at San Antonio, San Antonio, TX 78249, USA*
[8]*Université de Toulouse – UPS – OMP – IRAP, F-31400 Toulouse, France*
[9]*CNRS – IRAP, F-31028 Toulouse cedex 4, France*
[10]*Belgian Institute for Space Aeronomy, BIRA-IASB, B-1180 Brussels, Belgium*
[11]*Max-Planck-Institut für Sonnensystemforschung, D-37077 Göttingen, Germany*

ABSTRACT

As the spin axis of comet 67P/Churyumov–Gerasimenko (67P) is not normal to the orbital plane, 67P has strong seasonal changes in the illumination conditions on the nucleus' surface, with a short and intense summer in the Southern hemisphere. We have been monitoring these seasonal variations in the gas coma with the *Rosetta* Orbiter Spectrometer for Ion and Neutral Analysis (ROSINA) instrument suite aboard the ESA's *Rosetta* spacecraft. *Rosetta* followed 67P from its rendezvous in 2014 August, from a distance of almost 3.5 au to Sun, through perihelion at 1.24 au, and away from Sun again. In this study, we present the change of outgassing pattern during the 2016 March equinox based on measurements acquired with the ROSINA instruments: while H_2O, O_2 and NH_3 abundances rapidly decreased during this period, CO_2, CO, H_2S, CH_4 and HCN abundances decreased much less and showed a strong south–north heterogeneity for the whole period, thus not following Sun. Sublimation temperatures of the pure ices are found to be uncorrelated with the slope of the decrease for the minor species. This can be interpreted as a consequence of two different ice phases, water ice and CO_2 ice, in which the minor species are embedded in different relative abundances.

Key words: comets: individual: 67P/Churyumov–Gerasimenko.

1 INTRODUCTION

Comet 67P/Churyumov–Gerasimenko (hereafter 67P) was accompanied by the European Space Agency's *Rosetta* spacecraft for more than 2 yr along its trajectory around Sun. During this period, the comet crossed equinox for the first time in 2015 May, passed perihelion in 2015 August, and the second equinox in 2016 March, a few months before the mission was concluded with a final descent

on the nucleus of the comet. On board was ROSINA, the *Rosetta* Orbiter Spectrometer for Ion and Neutral Analysis instrument suite, built to monitor composition and abundance of the volatiles in the coma of the comet (Balsiger et al. 2007). ROSINA consisted of a pressure sensor and two complementary mass spectrometers, which together were well suited for this task.

67P has a changing rotation period (Keller et al. 2015) around a rotation axis tilted with respect to the orbit plane (Sierks et al. 2015). Hence, the illumination conditions on the nucleus surface are constantly changing in direction as well as in intensity given the variation in heliocentric distance from perihelion at 1.24 au to

⋆ E-mail: sebastien.gasc@space.unibe.ch

aphelion at 5.68 au. Summer on the Southern hemisphere is short and intense; summer on the Northern hemisphere is the opposite. This leads to strong seasonal heterogeneities of the volatiles in the coma, which was already observed early in the mission (Hässig et al. 2015; Le Roy et al. 2015). Given the strong asymmetries observed from north to south, it becomes especially interesting to track some of the major volatiles across equinox, when both hemispheres change season. The comet has been shown to be quite heterogeneous in its morphological features on the surface (Thomas et al. 2015; El-Maarry et al. 2016). However, deriving internal structure (Weissman 1986) and associated composition and heterogeneities in the sub-surface ices remain very difficult (Fulle et al. 2016). One reason for this is the build-up of a thermally insulating dust cover due to the sublimation of volatiles (Gortsas et al. 2011). Several mechanisms of the outgassing process have been discussed in the literature, including stratification of the ices based on their volatility including transport and re-condensation inside the nucleus, sublimation from the crystalline and from amorphous ices as well as from clathrates (Prialnik, Benkhoff & Podolak 2004; Marboeuf & Schmitt 2014; Lectez et al. 2015; Rubin et al. 2015; Mousis et al. 2016). One of the main goals of the *Rosetta* mission was hence to study the development of cometary activity and the processes in the surface layer of the nucleus (Glassmeier et al. 2007). The rapid changes in the illumination conditions over a moderately short-time period during the outbound equinox in 2016 March – when *Rosetta* spent time close to the nucleus – and associated variations in the distributions of the volatiles in the coma can add crucial information to the understanding of a comet's activity. The measurements obtained by ROSINA provide boundary conditions for deriving surface outgassing (Fougere et al. 2016; Marschall et al. 2016) and outgassing properties derived from numerical models of the nucleus interior and corresponding ices (Davidsson & Gutiérrez 2005; Rosenberg & Prialnik 2009; Marboeuf & Schmitt 2014). Section 2 of this paper presents a short description of the ROSINA instrument suite, followed by the details of the data treatment of the pressure sensor and both mass spectrometers. The obtained measurements are shown in Section 3 and our conclusions follow in Section 4.

2 MATERIALS AND METHODS

2.1 Instrument descriptions

ROSINA consists of the Comet Pressure Sensor (COPS) and two mass spectrometers, the Double Focusing Mass Spectrometer (DFMS) and the reflectron-type time-of-flight (RTOF) mass spectrometer. The three instruments work together to provide absolute density measurements of the major and minor volatiles in the coma of 67P.

In this study, we use data from all three instruments. It is therefore important to keep in mind that they all detect volatile neutral species, but that there are some important differences on how they measure. All three sensors ionize neutral particles by electron impact. However, their electron energies are different: 70, 45 and 0–150 eV for RTOF, DFMS and COPS, respectively. Whereas COPS measures the total neutral density every 2 s, but transmits data in a normal mode only every minute, RTOF collects one spectrum in 100 μs, but then accumulates 2 million spectra before the accumulated spectrum is transmitted. DFMS has to measure at integer mass numbers sequentially with an integration time of 20 s which yields 50 min for a full spectrum, including overhead for voltage stepping.

While COPS measures the combined density of all the species and does not separate masses, RTOF has a mass resolution $m/\Delta m$

of 500 and a mass range in the mode used for these measurements from 1 to 120 u, and DFMS has a mass resolution of $m/\Delta m \approx$ 9000 (at FWHM and mass 28 u) covering mostly masses from 13 to 100 u. RTOF is operated in a counting mode, while DFMS measures in an analogue mode the charge deposited from the MCP on to the anode. COPS measures directly the ion current. Sensitivity for RTOF and COPS depends mainly on the ionization cross-section of the different species, while DFMS has a mass-sensitive transmission and adjustable detector gain, which has to be taken into account. For more details, the reader is referred to Balsiger et al. (2007) and Scherer et al. (2006).

2.2 Data treatment

The RTOF data in this study were acquired with the storage source, designed to study neutrals (Balsiger et al. 2007). The data reduction is similar to that described in Gasc et al. (2017) and consists of (i) the correction of the ADC pattern for each spectrum individually, (ii) the application of the mass scale for each spectrum, (iii) the fitting and the numerical integration of each peak of interest, here H_2O and CO_2, and (iv) the scaling of the RTOF relative densities to the COPS measured absolute density values. Additionally, the first 30 min after each spacecraft manoeuvre has been systematically removed to minimize the impact of the outgassing of the ion source following the switch ON and heating up of RTOF.

The DFMS data in this study were acquired in a high-resolution mode (Balsiger et al. 2007). The data reduction process is the same as presented in Le Roy et al. (2015) and Calmonte et al. (2016) and consists of (i) MCP-related intensity correction, (ii) a mass calibration, (iii) the determination of the peak area per spectrum and per species and (iv) the conversion to number density for each species. For (iii), an automatic analysis software described in Calmonte et al. (2016) has been used to determine the peak area corresponding to CH_4, NH_3, H_2O, HCN, CO, O_2, H_2S and CO_2. The well-known contribution of CO from fragmentation of CO_2 has been subtracted from the CO signal to leave only cometary parent CO. The conversion to density (iv) is based on scaling the DFMS relative abundances measurements to the measured COPS total density shown in Fig. 1 as described in Gasc et al. (2017).

2.3 Observation period

The measurements discussed in the following were obtained with ROSINA during the extension of the *Rosetta* mission between 2016 January 1 and August 1, i.e. at heliocentric distances increasing from 2.0 to 3.5 au. The total density derived from the COPS measurements as well as some relevant orbital parameters of 67P and *Rosetta* during this time period are given in Fig. 1.

The chosen time frame covers the outbound equinox that occurred on 2016 March 21 at a heliocentric distance of 2.63 au. Coincidently, this distance matches the water iceline (or water condensation front), located around 2.7 au (Jewitt et al. 2007). During the studied period, the mean cometary activity decreased with distance as expected compared to perihelion, allowing the *Rosetta* spacecraft to get closer to the nucleus, from 90 to 7 km from the comet centre. Unfortunately, no ROSINA data are available for the interval 2016 March 23–2016 April 27 due to a tail excursion that brought *Rosetta* to a distance of 1000 km from the nucleus. Apart from this excursion, *Rosetta* remained mostly in a terminator orbit and studied the nucleus of 67P with a nadir off-pointing most of the time smaller than 10°. In particular, fast slews and large off-pointing angles can lead to increased release of volatiles trapped
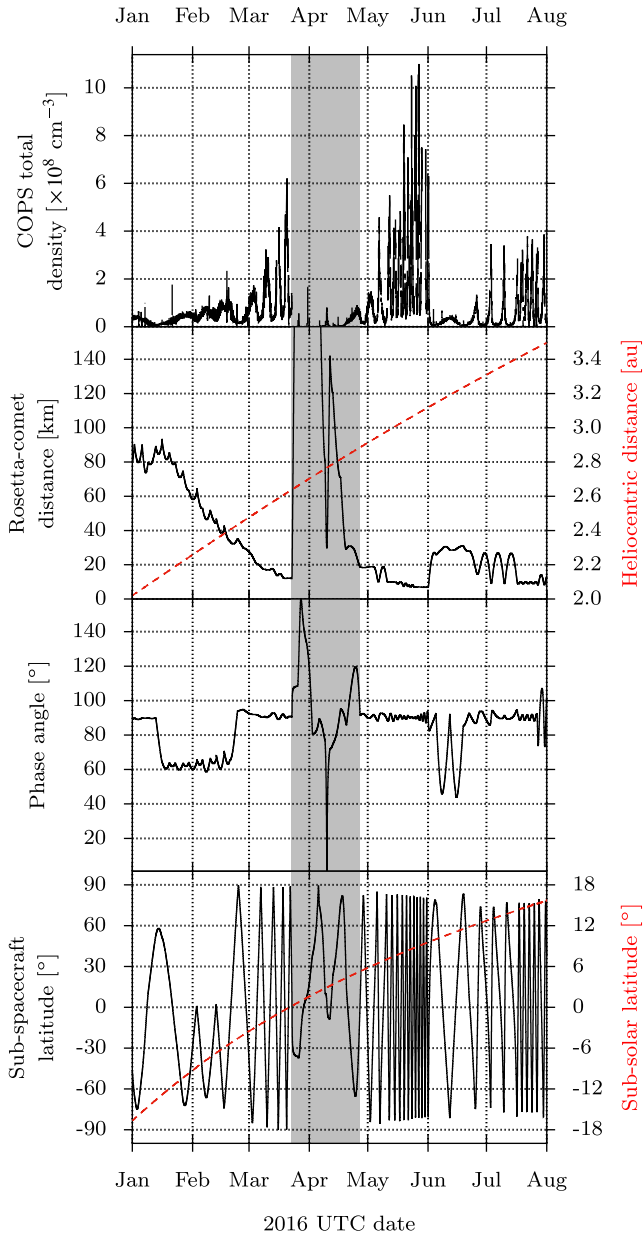
Figure 1. Top panel: COPS density. Second panel: distance from *Rosetta* to the nucleus centre (black) and heliocentric distance (dashed red). Third panel: phase angle. Bottom panel: sub-spacecraft latitude (black) and sub-solar latitude (dashed red). The period in grey corresponds to the tail excursion (2016 March 23–2016 April 27) when no measurements were acquired with the ROSINA mass spectrometers as the densities at these distances were too low.

on spacecraft surfaces that suddenly get illuminated and heat up. Furthermore, a fast-changing viewing geometry can affect the derived abundance ratios, especially in the case of DFMS, which measures each integer mass/charge ratio sequentially. As a consequence, time-periods with large slews have been removed from our analysis.

3 RESULTS

The time evolution of eight species measured by RTOF (H_2O and CO_2) and DFMS (CH_4, NH_3, H_2O, HCN, CO, O_2, H_2S and CO_2) is presented in this section. Table 1 summarizes the masses of these

Table 1. Average abundances relative to H_2O of the species studied in this work, for the periods 2016 January–April (2.0–2.7 au, middle column) and 2016 June–August (3.1–3.5 au, rightmost column). Species are sorted according to their abundance to H_2O for the later period.

Molecule	Abundance to H_2O pre-equinox (2.0–2.7 au)	Abundance to H_2O post-equinox (3.1–3.5 au)
CO_2	$(3.69 \pm 0.14) \times 10^{-1}$	3.31 ± 0.09
H_2O	1.00	1.00
CO	$(5.17 \pm 0.15) \times 10^{-2}$	$(5.23 \pm 0.12) \times 10^{-1}$
H_2S	$(3.77 \pm 0.10) \times 10^{-2}$	$(3.00 \pm 0.06) \times 10^{-1}$
CH_4	$(7.09 \pm 0.38) \times 10^{-3}$	$(1.08 \pm 0.03) \times 10^{-1}$
HCN	$(5.45 \pm 0.16) \times 10^{-3}$	$(4.97 \pm 0.11) \times 10^{-2}$
O_2	$(1.21 \pm 0.02) \times 10^{-2}$	$(1.97 \pm 0.03) \times 10^{-2}$
NH_3	$(3.78 \pm 0.13) \times 10^{-4}$	$(1.32 \pm 0.13) \times 10^{-4}$

species and provides abundances relative to H_2O averaged over the pre-equinox period (2.0–2.7 au) and the post-equinox period (3.1–3.5 au) described in Section 2.3. As ROSINA measured abundances at the location of the spacecraft, these densities of course scale with cometocentric distance. We therefore have multiplied the measured densities with r^2, the squared distance of the *Rosetta* spacecraft to the nucleus centre, to compensate for the radial decrease of the density, an approximation consistent with recent modelling efforts of the neutral gas environment (Bieler et al. 2015b; Fougere et al. 2016).

3.1 RTOF

The time evolutions of the H_2O and CO_2 densities measured by RTOF are presented in Fig. 2 and cover the time period from 2016 January to June. After 2016 June, the RTOF observation times were reduced due to power limitations.

Two different trends can be observed in the RTOF data. On the one hand, CO_2 abundance decreases relatively slowly as a function of the comet's distance from Sun, while showing large variations with changing sub-spacecraft latitude. On the other hand, H_2O shows small variations with sub-spacecraft latitude but a significant decrease with the increasing heliocentric distance, correlated with the sub-solar latitude.

The anticorrelation of CO_2 with the sub-spacecraft latitude already observed by RTOF before perihelion (Mall et al. 2016) was still clearly visible after perihelion, independent of the outbound equinox. On a shorter time-scale, the high-time resolution of RTOF (200 s) translates to a high-spatial resolution in the CO_2 time series, where diurnal variations are as well still visible and similar to measurements earlier in the mission (see Fig. 3).

To a lesser extent, the RTOF H_2O measurements show the anticorrelation with the sub-spacecraft latitude observed after the inbound equinox; before the inbound equinox, water molecules were emanating more abundantly from the Northern hemisphere, which was translated into a clear correlation with the latitude (Hoang et al. 2017). The sub-solar latitude changed slowly reaching about 16° north by the end of July. This is clearly different from the situation we had at the beginning of the mission in 2014 September when Sun was almost at 50° north for the same heliocentric distances. Accordingly, while the heterogeneity for water between north and south did change after equinox, it did not reach the situation where much more water was released from the Northern hemisphere than from the south as in 2014 September (Hässig et al. 2015). The pattern we see is rather flat, indicating that water is following the
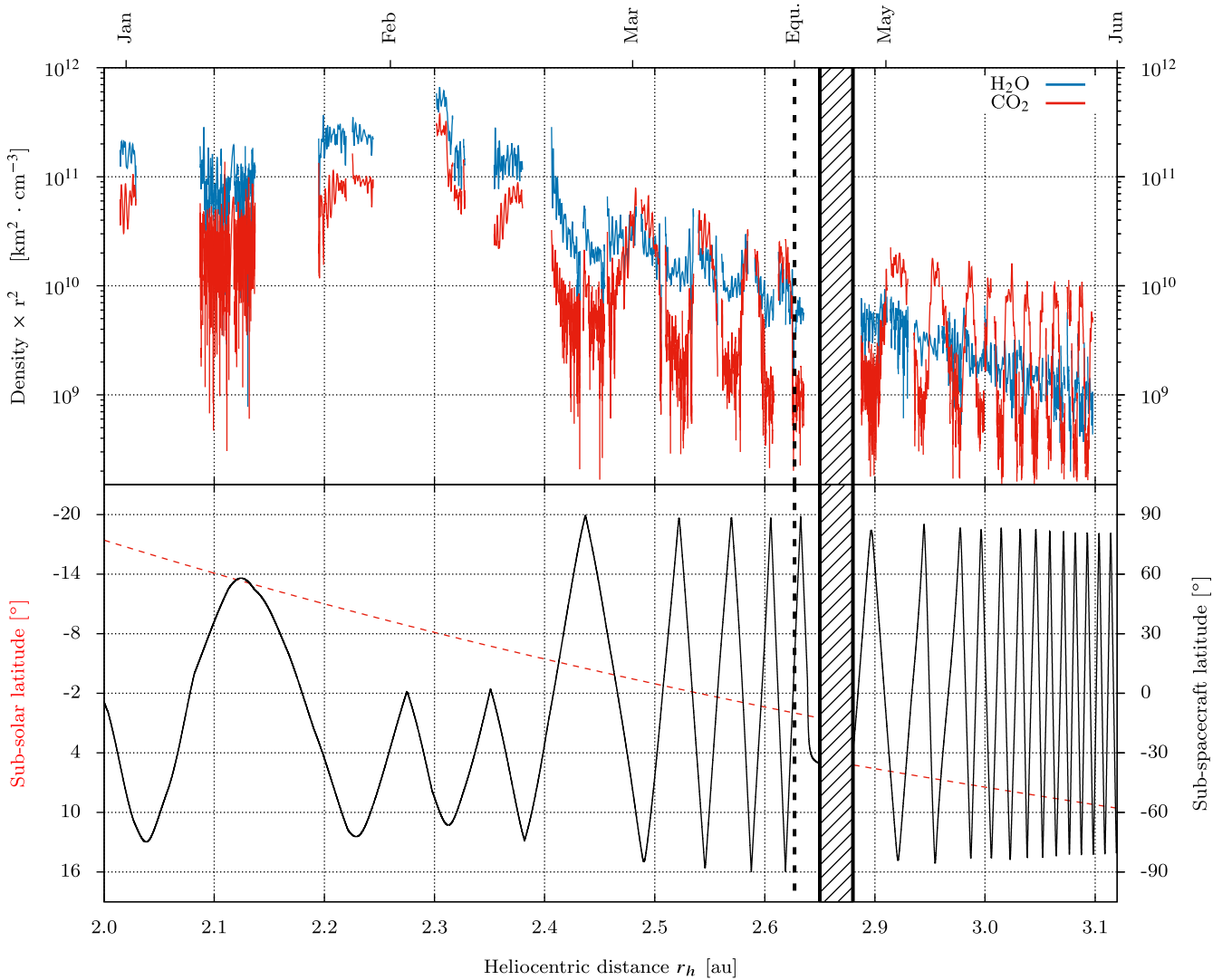
Figure 2. Top panel: evolution of H_2O (blue) and CO_2 (red) densities measured by RTOF between 2016 January and June, corresponding to a heliocentric distance ranging from 2.0 to 3.1 au. The densities derived from the RTOF measurements have been multiplied by r^2, with r the distance from the *Rosetta* spacecraft to the centre of the comet, to compensate for the decrease of the atmospheric density which follows a r^{-2} law. Bottom panel: sub-solar latitude (dashed red) and sub-spacecraft latitude (black).

sub-solar latitude to the equator and then beyond. This can be seen if looking carefully at Fig. 3, where water actually peaks around 0° latitude in 2016 May.

3.2 DFMS

The time evolutions of the densities measured by DFMS for CH_4, NH_3, H_2O, HCN, CO, O_2, H_2S and CO_2 are shown in Fig. 4. The DFMS data from 2016 May (heliocentric distance from 2.91 to 3.12 au) are not shown due to the small amount of data points for the studied species in this period.

DFMS confirms the global trend observed with RTOF for H_2O and CO_2 and allows distinction of two populations: species such as H_2O, O_2 and NH_3 show less difference in their north/south abundances than CO_2, CO, H_2S, CH_4 and HCN, which stay high over southern latitudes and are significantly lower at northern latitudes. These two populations are in agreement with the results shown by Luspay-Kuti et al. (2015), except for HCN, which in 2014 showed a significantly better correlation with H_2O than with CO_2. To quantify

the different behaviour, we have fitted the data for latitudes $>30°$ (north) and $<-30°$ (south) with a power law to the heliocentric distances. The power-law indices α are given in Table 2 and the corresponding plots can be found in the Appendix. No correlation of the power-law indices α with the sublimation temperature of pure ices is observed (see Fig. 5). We have also calculated the mean ratio $R_{S/N}$ between south and north abundances for 2016 March and July. The generally steeper decrease with heliocentric distance in the south compared to north is most probably an effect of the change in sub-solar latitude: more northern parts and less southern parts are illuminated with time and therefore with heliocentric distance. Accordingly, the ratios between south and north are smaller in 2016 May than in 2016 March.

The strong heterogeneity of the coma can be mostly explained by solar insolation. In addition, however, some inhomogeneity of the nucleus surface has to be taken into account (Fougere et al. 2016), which is mostly attributed to dust coverage in the north and fresher material in the south. Fig. 6 illustrates the changes in abundance with the sub-spacecraft latitude for 2016 March. No difference between
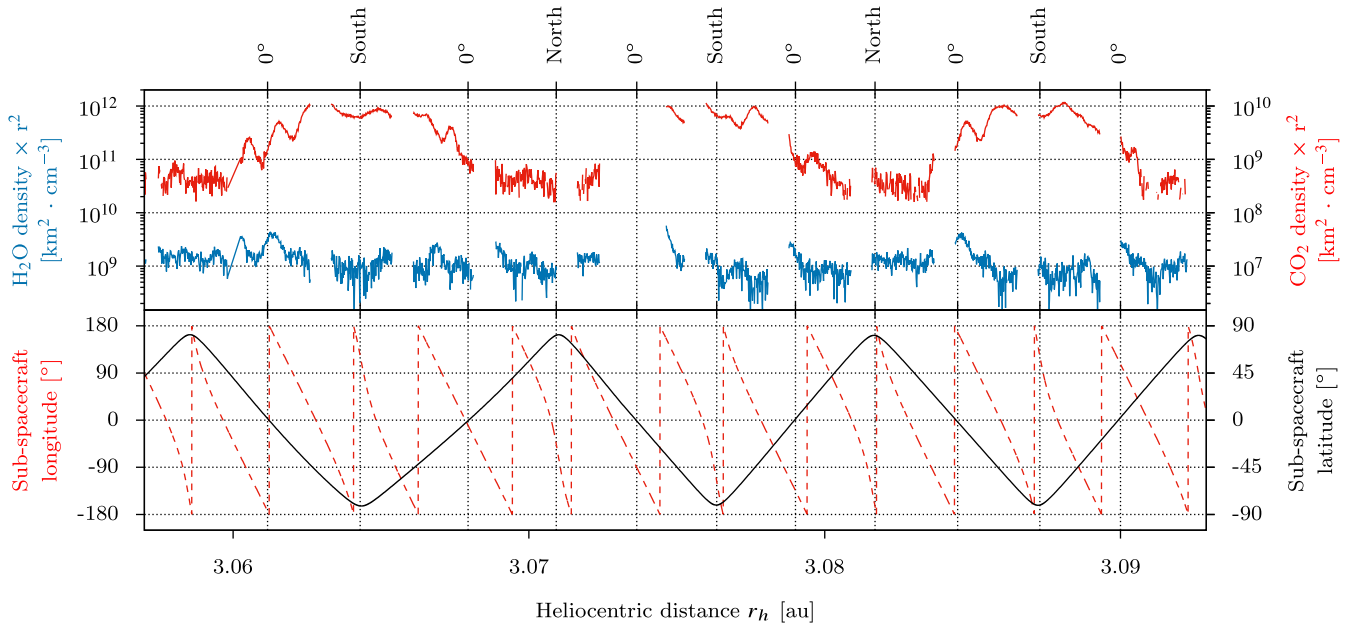
Figure 3. Top panel: evolution of H_2O (blue) and CO_2 (red) densities measured by RTOF between 2016 May 22 and 2016 May 28 (heliocentric distance from 3.057 to 3.093 au). Bottom panel: sub-spacecraft longitude (red) and sub-spacecraft latitude (black), with minimum and maximum sub-spacecraft latitudes and crossings of the equator indicated on top.

measurements acquired at dawn (local time close to 6:00) and at dusk (local time close to 18:00) can be observed. During and after the outbound equinox, the variations between the two hemispheres of H_2O, together with O_2 and NH_3, are much weaker than before the outbound equinox, but the long-term trend reveals a considerable decrease in the water sublimation. This decrease is due mostly to the increasing heliocentric distance, as the period around equinox coincided with the crossing of the snow line of water.

O_2 was known to follow H_2O in the coma of comet 67P/Churyumov–Gerasimenko before the inbound equinox with ratios of 0.01–0.1 compared with H_2O and a mean O_2/H_2O ratio from 2014 September to 2015 April of 0.0380 ± 0.0085 (Bieler et al. 2015a). After the outbound equinox, these ratios remained similar (see Table 1), with a temporal evolution of O_2 following closely the evolution of H_2O. Fig. 7 shows correlation plots for all species with respect to H_2O and CO_2 for two periods, near and post equinox (2.4–2.7 and 3.2–3.5 au, respectively). The O_2–H_2O correlation is clear for both periods. On the short term H_2O and NH_3 correlate well, but on the long term, between 3.2 and 3.5 au and after the outbound equinox, the evolution of NH_3 is flatter with distance to Sun. Most other species show very little correlation with H_2O, although some intrinsic correlation is given by the change in heliocentric distance over the periods, which affects all species, but not all alike. CO_2 and H_2O do not correlate, whereas CO, CH_4, HCN and H_2S correlate rather well with CO_2.

The species varying strongly with the sub-spacecraft latitude during equinox, i.e. CO_2, CO, H_2S, CH_4 and HCN, all had very similar trends, especially before 2016 April and the exchange of seasons between both hemispheres: detected more abundantly in the Southern hemisphere, the outgassing of these molecules decreased slowly and regularly on the long term, following the increasing heliocentric distance and thus the decrease of the solar input. These similarities were observed likely post-equinox, with a slight difference regarding H_2S, CH_4 and HCN which locally resembled water, around

3.18 au, i.e. with higher abundances at sub-spacecraft latitudes close to $0°$.

4 DISCUSSIONS AND CONCLUSIONS

ROSINA, RTOF and DFMS monitored a set of eight molecules, including CH_4, NH_3, H_2O, HCN, CO, O_2, H_2S and CO_2, for several weeks throughout the outbound equinox of comet 67P. *Rosetta* orbited the comet in the terminator plane and hence covered both hemispheres of the comet repetitively. This provided the unique possibility to compare not only the different outgassing patterns of these molecules but also their temporal variations as the illumination of the nucleus was changing. Strong north/south heterogeneities have been observed, similar to observations early in the mission which were also performed beyond 3 au (Hässig et al. 2015), although in the pre-perihelion period the total outgassing was always dominated by H_2O (Fougere et al. 2016). Water seems to follow the sub-solar latitude, which was expected given its rather high sublimation temperature (Hansen et al. 2016). CO_2 does not trend the same way, as the Southern hemisphere remained its main source and, hence, towards the end of the mission, the southern, winter hemisphere dominated the outgassing of 67P through CO_2.

The general decrease over the period in abundances varies greatly from species to species. It does not follow the sublimation temperatures of pure ices (Table 2). The smallest decrease is seen in CO_2, which exhibits at the same time the highest variation between north and south during equinox. The power law with heliocentric distance is roughly -2 for the Southern hemisphere and -0.7 for the northern part. That means the outgassing of CO_2 is not an instant response to solar illumination, but rather due to heat diffusion into and thermal inertia of deeper layers below the surface. On the other hand, H_2O seems to follow the subsolar latitude. The power law with an exponent of -7 and -11 for north and south, respectively, shows that temperatures of the nucleus are below the sublimation temperature of water on both hemispheres, even at subsolar
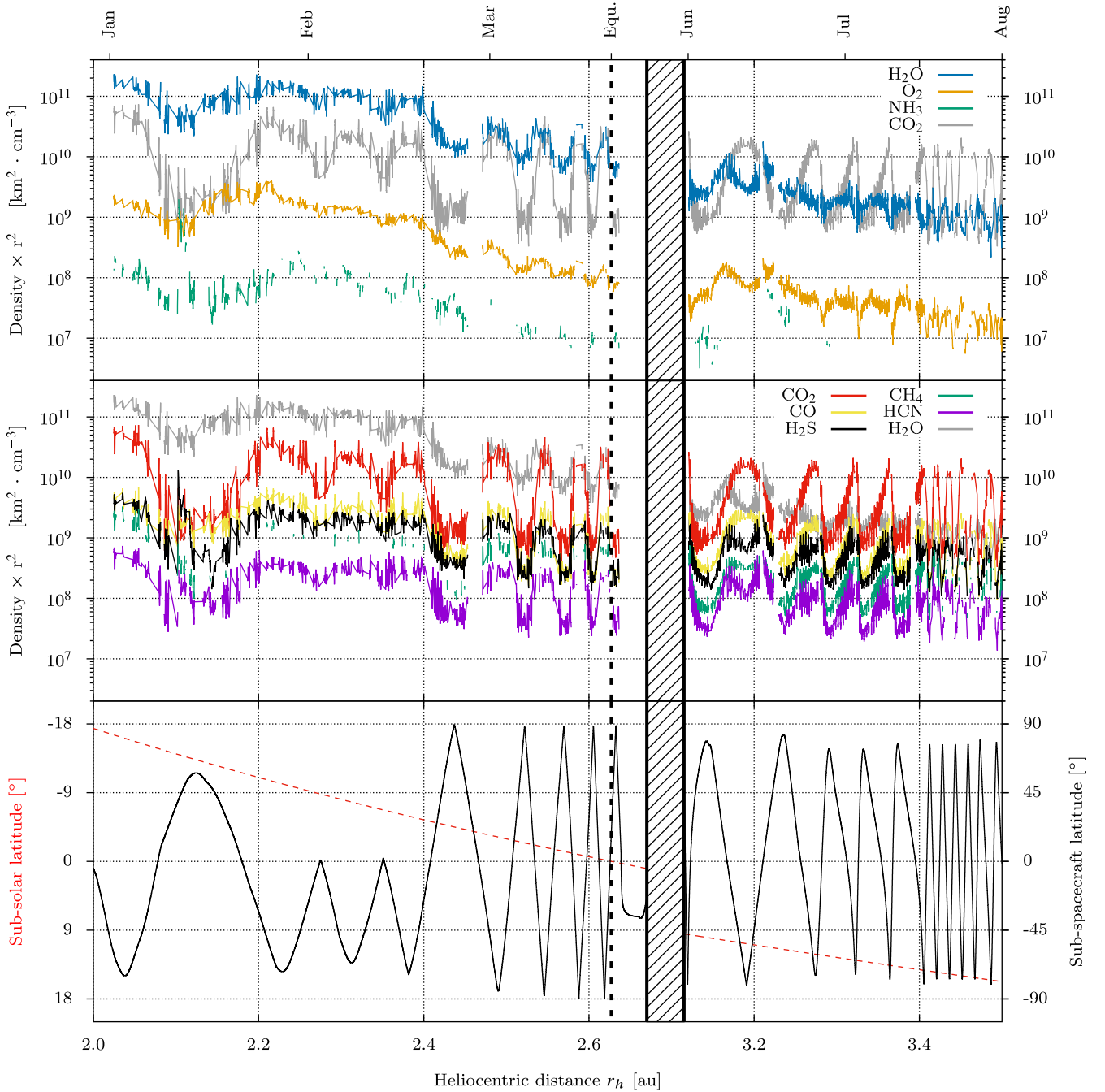
Figure 4. Evolution of the most abundant species detected by DFMS between 2016 January and August, at heliocentric distances ranging from 2.0 to 3.5 au. In the same way as for the RTOF measurements, the DFMS densities have been multiplied by r^2, the squared distance from the *Rosetta* spacecraft to the cometary nucleus. Top panel: H_2O, O_2 and NH_3; CO_2 is added in grey for comparison. Middle panel: CO_2, CO, H_2S, CH_4 and HCN; H_2O is added in grey for comparison. Bottom panel: sub-spacecraft latitude (black) and sub-solar latitude (red).

latitudes. O_2 is a special case. Its exponents of -6.7 to -8.9 for the power law are close to the water, although its volatility is very high, second only to CO, confirming the close relationship between water and O_2 (Bieler et al. 2015a). Molecular oxygen, O_2, which, according to Bieler et al. (2015a), hints at formation inside pre-solar water ices by irradiation processes, leads to a close relation between the two molecules (cf. Mousis et al. 2016) despite grossly different sublimation temperatures (see Table 2). If we include earlier findings, e.g. the lack of correlation of molecular nitrogen, N_2, with water (Balsiger et al. 2015) and the correlation of O_2 with water, we end

up with two species, N_2 and O_2, with almost indistinguishable desorption patterns as a function of temperature (Collings et al. 2004) but vastly different outgassing profiles measured at the comet.

After equinox, CO_2 remained dominant in the Southern hemisphere, more abundant than on the better illuminated Northern hemisphere. The same applied to CO, H_2S, CH_4 and HCN, although some of them with a less strong north/south variation in the measured density. According to Collings et al. (2004), species that are co-deposited with water at cold temperatures, where water is amorphous, desorb in three steps: the first step is close to the

Table 2. Other properties of the species studied in this work. Sublimation temperatures T_{sub} are derived from Fray & Schmitt (2009) (sublimation from pure ices). The power-law indices α were calculated for latitudes $>30°$ (north) and $<-30°$ (south), via a fit of the data with a power law to the heliocentric distances. Mean ratios $R_{S/N}$ between north and south abundances for 2016 March and July are given in the two rightmost columns. Species are sorted according to their slope α – south with heliocentric distance for the Southern hemisphere.

Molecule	Mass [u/e]	T_{sub} [K]	α – North	α – South	$R_{S/N}$ – March	$R_{S/N}$ – July
H_2O	18.01	144	-7.32 ± 0.04	-11.42 ± 0.05	2.68 ± 0.06	0.62 ± 0.02
O_2	31.99	30	-6.66 ± 0.05	-8.92 ± 0.05	1.72 ± 0.04	0.81 ± 0.01
NH_3	17.03	102	-4.88 ± 0.18	–	–	–
H_2S	33.99	80	-1.74 ± 0.05	-3.59 ± 0.03	4.66 ± 0.11	2.31 ± 0.04
CH_4	16.03	36	-2.26 ± 0.07	-3.21 ± 0.03	–	3.88 ± 0.10
HCN	27.01	126	-1.57 ± 0.05	-2.76 ± 0.03	4.80 ± 0.18	2.72 ± 0.06
CO_2	43.99	86	-0.68 ± 0.05	-2.18 ± 0.04	22.20 ± 0.66	11.53 ± 0.21
CO	27.99	28	-2.21 ± 0.05	-1.83 ± 0.03	9.98 ± 0.24	6.07 ± 0.09
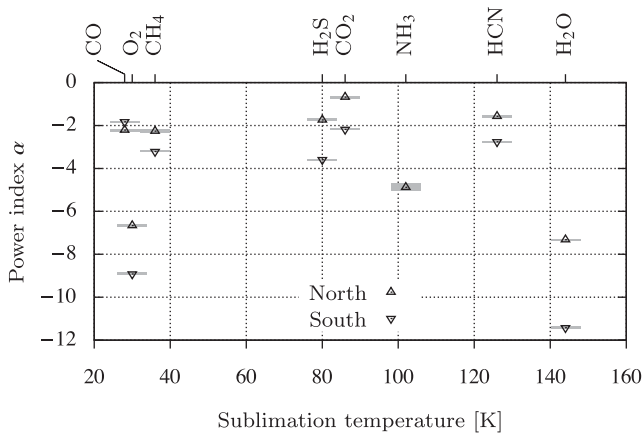
Figure 5. Power-law indices α versus sublimation temperature, for the studied species and for latitudes $>30°$ (north) and $<-30°$ (south). The grey boxes represent the error on α.

sublimation temperatures of pure ices, the second step, which is the same for all species more volatile to water, happens at $\approx$120 K, where water converts from amorphous to crystalline (volcano desorption) and the third step happens at the sublimation temperature of water. The behaviour of the species studied here does not follow this scheme. There are clear differences in desorption patterns between species that cannot be explained by their volatility. For example, CH_4 (36 K) and HCN (126 K) have very different sublimation temperatures, but show very similar slopes with heliocentric distances. O_2 and CH_4 have very similar sublimation temperatures, but have completely different slopes. This cannot be explained by pure ices, but hints at mixtures of species and ice types. The heterogeneity seen in most species between north and south might have their origin in the hemispherical differences between the northern and southern surfaces of the comet. The intense summer in the south sets free fresh material and the outgassing of volatiles continuously sheds any accumulated dust mantle. Kramer et al. (2017) showed that sources of enhanced gas activity were correlated to the location of dust outbursts observed within 3 months around perihelion (2015 July–September). Furthermore, these gas sources remained active until the end of the mission, much longer compared to the dust outbursts that typically last for only a few minutes and dust itself appears to be dry (De Keyser et al. 2017). In the north, lower outgassing rates and back-fall of dust (Agarwal et al. 2016; Keller et al. 2017) possibly quench the outgassing rate. If such grains contain any volatiles such as water, outgassing from back-fall would

certainly be dominated by these species. Species of higher volatility would be long lost by the time of redeposition. Therefore, higher relative abundance of water is not in contradiction to the scenario proposed by Keller et al. (2017).

There exist models of desorption from cometary nuclei and laboratory experiments where species more volatile than water desorb and migrate outwards and inwards where they freeze out again (e.g. Mekler, Prialnik & Podolak 1990, and references therein; Notesco & Bar-Nun 2000, and references therein). However, most of the models and all of the experiments take into account much larger relative abundances of the minor species. In our data, relative abundances, except for CO_2, were all in the 1 per cent range before and around equinox and therefore very minor. It cannot be expected that pure ices of these minor species exist in the comet. Their sublimation temperature, with the exception of CO_2, may therefore be irrelevant because for desorption of a minor species in a matrix of volatiles and dust, van der Waals forces in the host matrix, which are different from the pure ices, are responsible. The continuous strong outgassing from the southern parts over many months and even years with very little water is probably indicative of CO_2 ice. CO_2 was found to be abundant in the coma over the Southern hemisphere already at the beginning of the *Rosetta* mission (Hässig et al. 2015) after the southern part had been in shadow for 5 yr. Experimentally, it has been shown by Fayolle et al. (2011) that with an intimate mixture of $H_2O:CO_2$ of 5:1, the topmost layer saturates quickly with H_2O molecules and the pores become void of more volatile species below the sublimation temperature of H_2O and the surface layer is then impenetrable for CO_2. This would suppress CO_2 outgassing quite rapidly, once the temperature of the surface layer is below the sublimation temperature of water. This clearly does not happen at the comet (Fig. 2). Our conclusion is that the ices cannot be intimately mixed, be it due to primordial separation or by evolution.

Therefore, a possible explanation for the observed sublimation temperature-independent diversity in desorption could be that minor species are partly embedded in CO_2 and partly in H_2O ices. Their different power laws with heliocentric distance are then indicative for the ratio between how much is embedded in CO_2 and are therefore co-desorbed with CO_2 and how much is embedded in water and is released by the volcano effect or by sublimation of water. Good examples are H_2S and HCN, which generally follow CO_2 (power-law indices of -1.57 to -3.59), but show some signature of the water release not seen in CO_2 like the double peak at, e.g. 3.18 au (Fig. 4). This means that the nucleus consists partly of CO_2 dominated ices, partly of H_2O dominated ones. If this is a primordial heterogeneity or due to differentiation because of
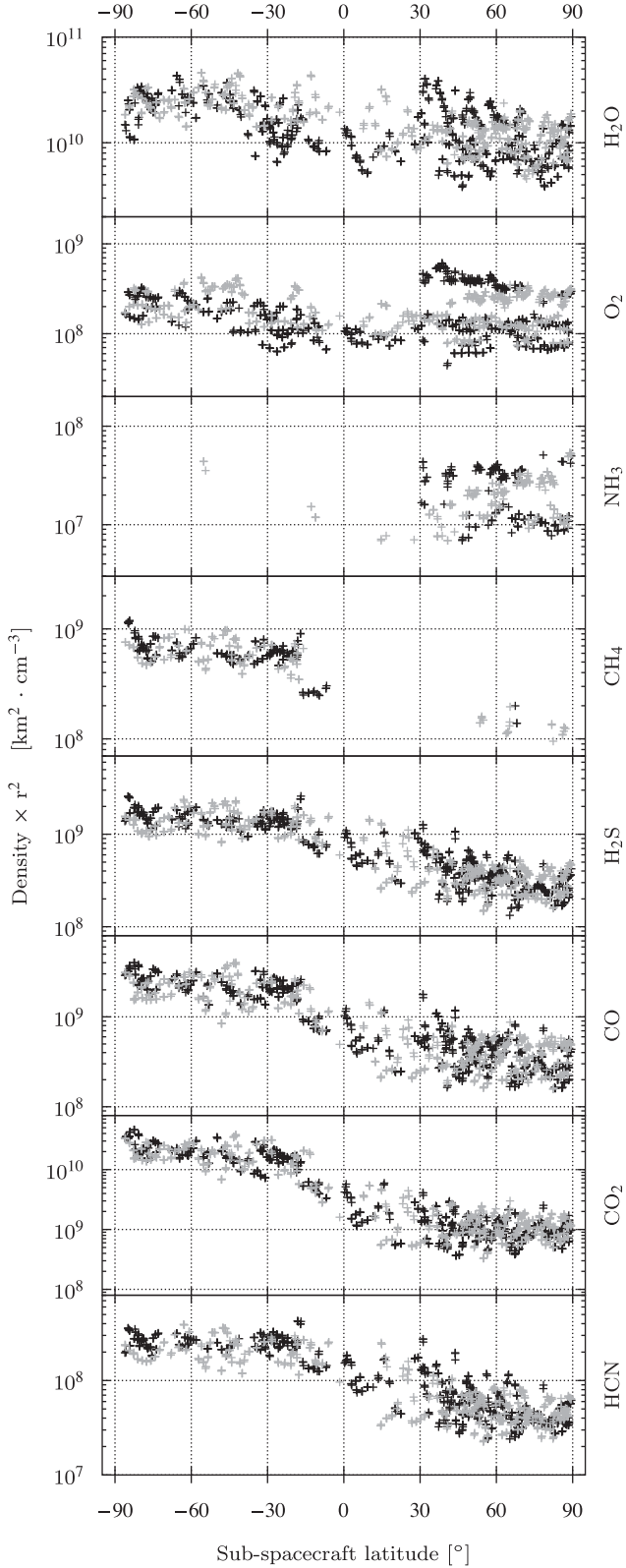
Figure 6. Evolution of the studied species with respect to the sub-spacecraft latitude for the time period 2016 February 19–2016 March 23 (2.40–2.63 au). Grey points represent measurements acquired at dawn (local time close to 6:00), whereas black points represent measurements acquired at dusk (local time close to 18:00).
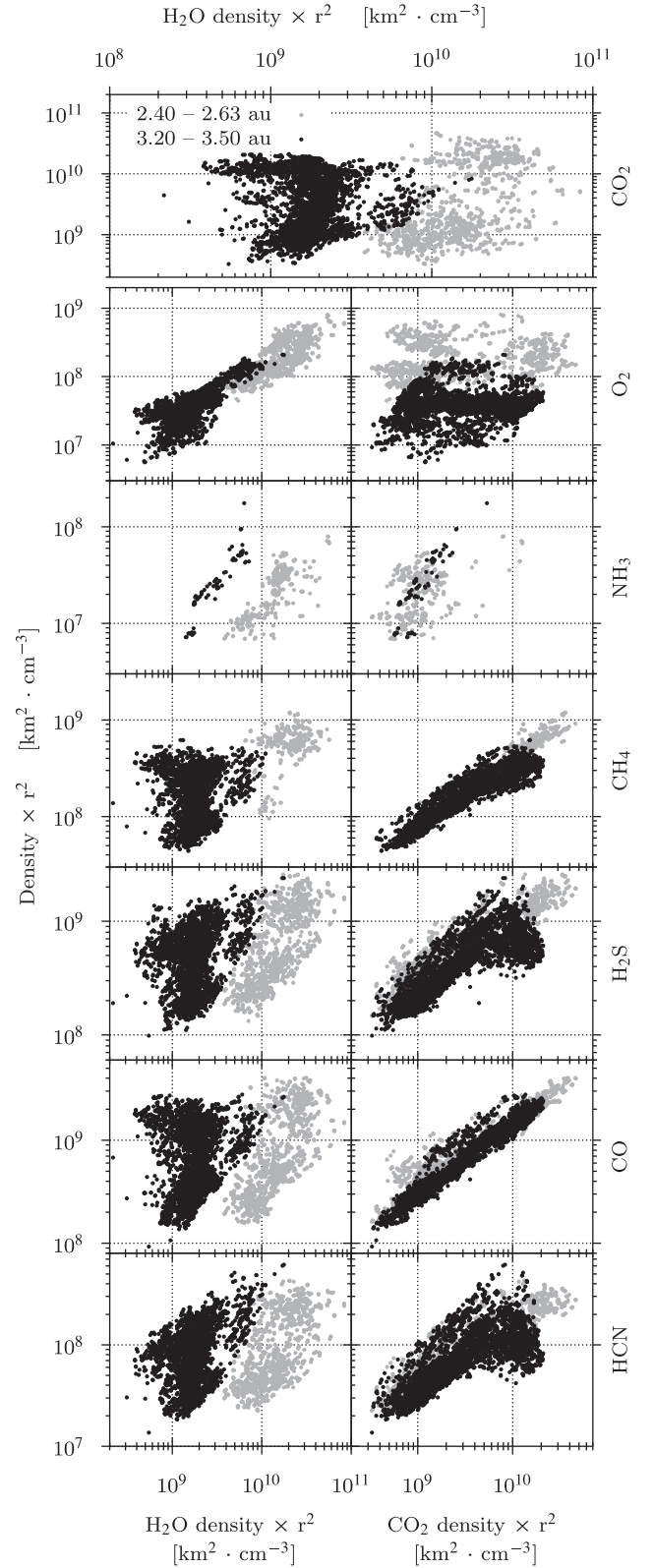
Figure 7. Top: scatter plot of CO_2 versus H_2O. Lower left graphs: scatter plots of the studies species versus H_2O. Lower right graphs: scatter plots of the studies species versus CO_2. The measurements shown here belong to the time period 2016 February 19–2016 March 23 (2.40–2.63 au, grey), and June 13–August 1 (3.20–3.50 au, black).

evolution is hard to say. There is, however, no indication that polarity of the species plays a role, as one might expect that polar species are more likely to be embedded in water and apolar ones in CO_2. Furthermore, also how each molecule is embedded in the ice, either through trapping, formation in the ice through radiation, grain-surface chemistry or refreezing, affects probably the structure and therefore the van der Waals forces in the matrix and the later desorption. Clearly, more laboratory work on low mixing ratios in H_2O and, in particular, CO_2 ice has to be done.

Before the end of the *Rosetta* mission, the comet transitioned to be dominated by highly volatiles. Towards outbound equinox in 2016 March at ≈ 2.6 au, the CO_2 abundance increased with respect to H_2O and, while the turnover was not instant, CO_2 became the dominant molecule in the coma of the comet, at least at the location of *Rosetta* in the terminator plane. This behaviour is associated with the low sublimation temperature and is in line with what has been observed at other comets, such as CO (possibly with contribution from CO_2) versus the water fragment OH at Hale-Bopp (Biver et al. 2002).

REFERENCES

Agarwal J. et al., 2016, MNRAS, 462, S78
Balsiger H. et al., 2007, Space Sci. Rev., 128, 745
Balsiger H. et al., 2015, Sci. Adv., 1
Bieler A. et al., 2015a, Nature, 526, 678
Bieler A. et al., 2015b, A&A, 583, A7
Biver N. et al., 2002, Earth Moon Planets, 90, 5
Calmonte U. et al., 2016, MNRAS, 462, S253
Collings M. P., Anderson M. A., Chen R., Dever J. W., Viti S., Williams D. A., McCoustra M. R. S., 2004, MNRAS, 354, 1133
Davidsson B. J. R., Gutiérrez P. J., 2005, Icarus, 176, 453
De Keyser J. et al., 2017, MNRAS, this issue
El-Maarry M. R. et al., 2016, A&A, 593, A110
Fayolle E. C., Öberg K. I., Cuppen H. M., Visser R., Linnartz H., 2011, A&A, 529, A74
Fougere N. et al., 2016, MNRAS, 462, S156
Fray N., Schmitt B., 2009, Planet. Space Sci., 57, 2053
Fulle M., Altobelli N., Buratti B., Choukroun M., Fulchignoni M., Grün E., Taylor M. G. G. T., Weissman P., 2016, MNRAS, 462, S2
Gasc S. et al., 2017, Planet. Space Sci., 135, 64
Glassmeier K.-H., Boehnhardt H., Koschny D., Kührt E., Richter I., 2007, Space Sci. Rev., 128, 1
Gortsas N., Kührt E., Motschmann U., Keller H. U., 2011, Icarus, 212, 858
Hansen K. C. et al., 2016, MNRAS, 462, S491
Hässig M. et al., 2015, Science, 347, aaa0276
Hoang M. et al., 2017, A&A, 600, A77
Jewitt D., Chizmadia L., Grimm R., Prialnik D., 2007, in Reipurth V. B., Jewitt D., Keil K., eds, Protostars and Planets V. Univ. Arizona Press, Tucson, p. 863
Keller H. U., Mottola S., Skorov Y., Jorda L., 2015, A&A, 579, L5
Keller H. U. et al., 2017, MNRAS, this issue
Kramer T., Läuter M., Rubin M., Altwegg K., 2017, MNRAS
Le Roy L. et al., 2015, A&A, 583, A1
Lectez S., Simon J.-M., Mousis O., Picaud S., Altwegg K., Rubin M., Salazar J. M., 2015, ApJ, 805, L1
Luspay-Kuti A. et al., 2015, A&A, 583, A4
Mall U. et al., 2016, ApJ, 819, 126
Marboeuf U., Schmitt B., 2014, Icarus, 242, 225
Marschall R. et al., 2016, A&A, 589, A90
Mekler Y., Prialnik D., Podolak M., 1990, ApJ, 356, 682
Mousis O. et al., 2016, ApJ, 823, L41
Notesco G., Bar-Nun A., 2000, Icarus, 148, 456
Prialnik D., Benkhoff J., Podolak M., 2004, in Festou M. C., Keller H. U., Weaver H. A., eds, Modeling the Structure and Activity of Comet Nuclei. Univ. Arizona Press, Tucson, p. 359
Rosenberg E. D., Prialnik D., 2009, Icarus, 201, 740
Rubin M. et al., 2015, Science, 348, 232
Scherer S. et al., 2006, Int. J. Mass Spectrom., 251, 73
Sierks H. et al., 2015, Science, 347, aaa1044
Thomas N. et al., 2015, Science, 347, aaa0440
Weissman P. R., 1986, Nature, 320, 242

APPENDIX: SUPPLEMENTARY MATERIAL

The densities of the eight studied molecules have been fitted using the non-linear least-squares Marquardt–Levenberg algorithm, for latitudes $>30°$ (north) and $<-30°$ (south), and based on the following power law:

$$n \cdot r^2 = C \cdot r_{\mathrm{h}}^{\alpha}$$

with n the density of the fitted species, r the distance of the *Rosetta* spacecraft to the nucleus centre, r_{h} the heliocentric distance, α the fitted power-law indices and C a constant parameter. The fit was done using logarithmic values to account for the small weight of the low densities on the y axis:

$$f_{\mathrm{fit}}(r_{\mathrm{h}}) = \alpha \cdot \log_{10}(r_{\mathrm{h}}) + \log_{10}(C)$$

The data points, their associated fit and the fitted value of α are shown in Figs A1 and A2.
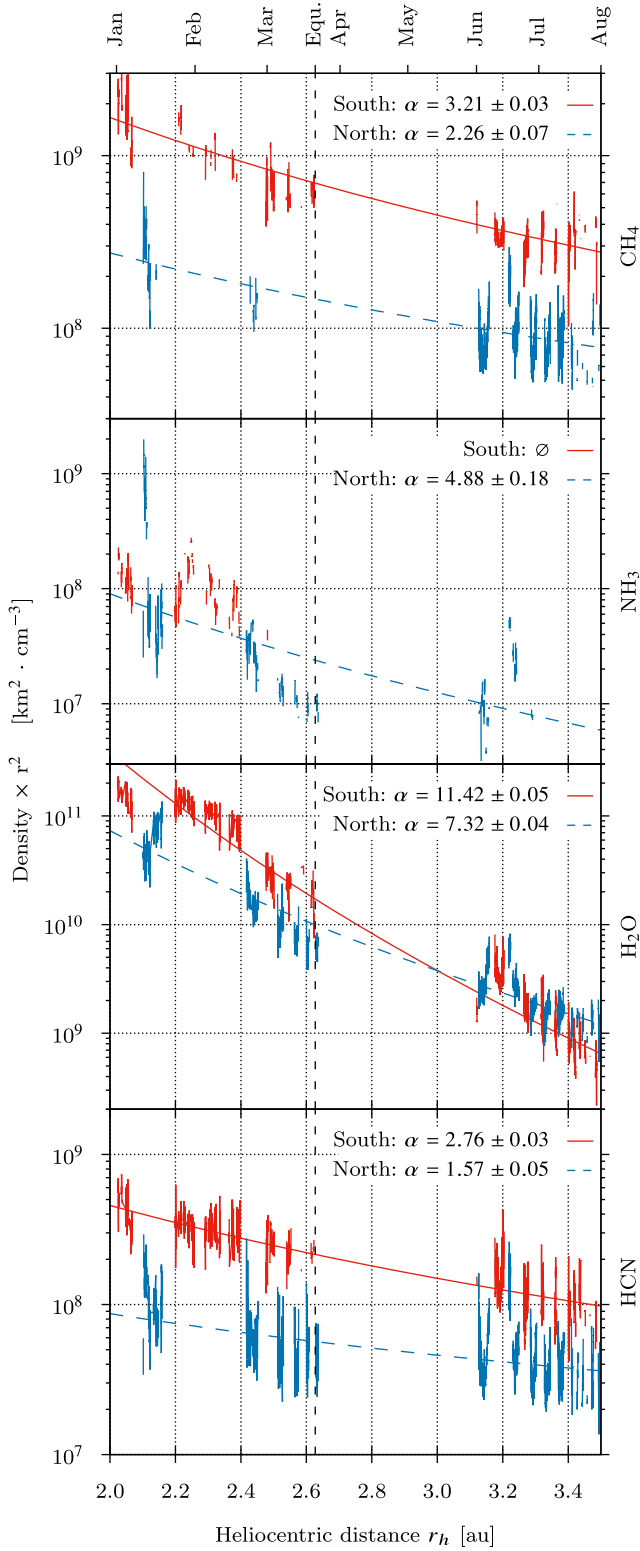
Figure A1. From top to bottom: densities ($\times r^2$) of CH_4, NH_3, H_2O and HCN, fitted with a power law to the heliocentric distance, for sub-spacecraft latitudes $>30°$ (north – dashed blue) and $<-30°$ (south – red).
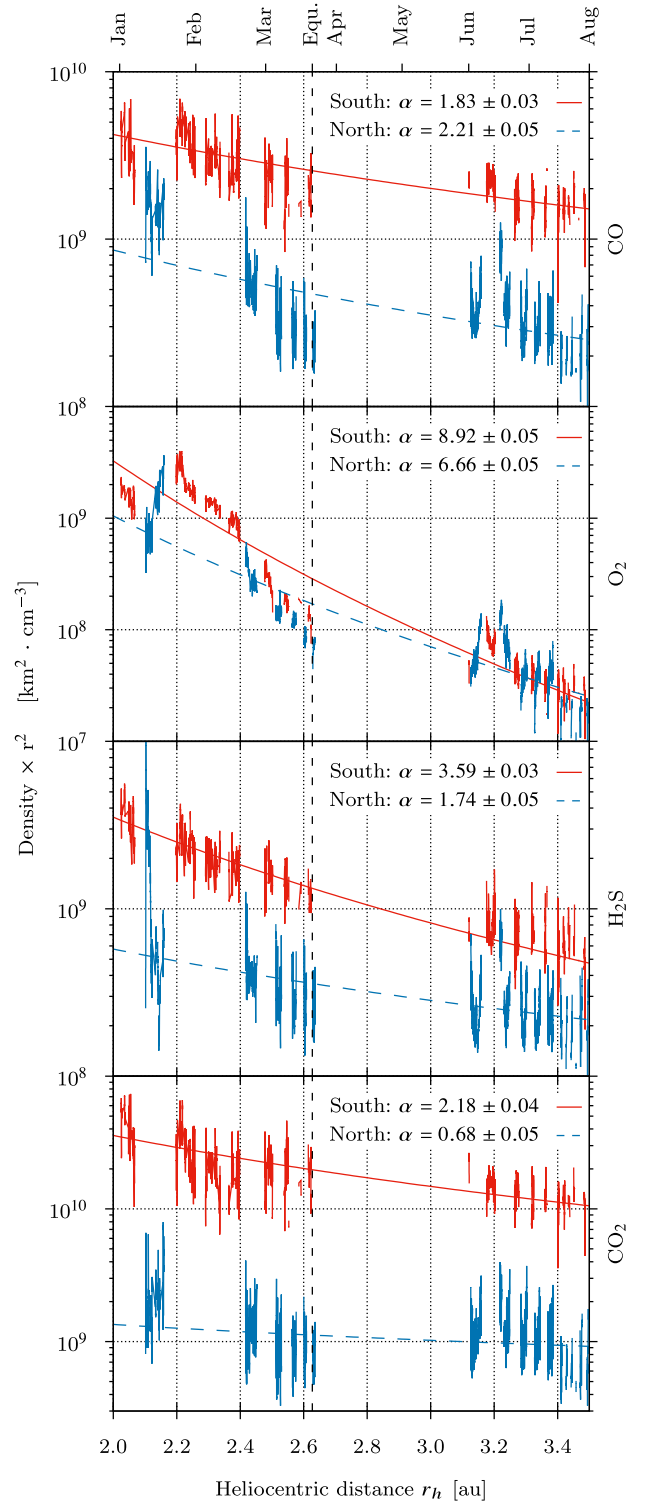

Figure A2. From top to bottom: densities ($\times r^2$) of CO, O_2, H_2S and CO_2, fitted with a power law to the heliocentric distance, for sub-spacecraft latitudes $>30°$ (north – dashed blue) and $<-30°$ (south – red).

This paper has been typeset from a TEX/LATEX file prepared by the author.